2018 IEEE 15th International Symposium on Biomedical Imaging (ISBI 2018)
April 4-7, 2018, Washington, D.C., USA

QUANTUM CASCADE LASER INFRARED MICROSCOPY DIFFERENTIATES MALIGNANT PHENOTYPES IN BREAST HISTOLOGY SECTIONS

Garrett Winkelmaier[1], Mina Khoshdeli[1], Qingsu Cheng[1], Alexander Borowsky[2], and Bahram Parvin[1]

[1]University of Nevada, Reno
Department of Electrical and Biomedical Engineering

[2]University of California, Davis
School of Medicine

ABSTRACT

Quantum Cascade Laser InfRared (QCL-IR) microscopy has the potential to emerge as a unique modality for the diagnostics of histology sections. A pilot experiment is designed to evaluate whether benign and malignant breast histology sections can be differentiated using chemical profiling and without the use of spatial information. The experiment consists of 22 independent samples that were randomly selected from paraffin-embedded blocks with an equal number of benign and malignant labels. Spectral data are normalized and then used for both visualization and classification. Visualization is based on consensus clustering of the spectral signature within each group of the benign or malignant phenotype. Classification has been evaluated with three methods of tree-based, convolutional neural networks, and an encoder module for compression followed by softmax classification. The latter has the best performance with using only 20% of the data for training to arrive at the classification accuracy of 100%. Direct analysis of the spectral signatures indicates that both malignant and benign samples express the similar spectral peaks; however, peaks corresponding to several nucleic acid sequences and protein groups are overexpressed in malignant tissues.

Index Terms— QCL-IR, spectral pathology, breast cancer, machine learning.

1. INTRODUCTION

Automated classification of histology sections has been advanced for a number of tumor types. Often, the methodologies are based on morphological characteristics using H&E stains and bright field imaging [1-3], where novel computational methods have been developed for spatial profiling of histology section terms of tumor grading, and cellular characterization and organization [3-6]. In this study, we have designed a pilot study to examine whether malignant breast histology can be classified using chemical imaging when imaged by mid-infrared microscopy. Accordingly, no spatial information is utilized, and classification is based strictly on pixels with hyperspectral signatures, which have been sampled randomly from each image. While contrast in H&E stained samples is provided by adding chemical stains, the contrast in QCL imaging spectroscopy is provided purely by the intrinsic chemical properties of the sample [7, 8] and in terms of spectra. The spectra (i) reflects the interaction of infrared radiation with molecular vibrations within the tissue to produce a unique signature; and (ii) contains absorption bands containing proteins, lipid, and carbohydrates. Utilizing spectral signatures to identify chemical differences between normal and diseased tissue has been referred to spectral histopathology (SHP)[9]. Our pilot study consists of a tumor microarray of benign and malignant breast histology samples to evaluate discrimination based on chemical signatures, where Figure 1 shows typical spectra with 226 channels from a single TMA. We outline our approach in terms of preprocessing and visualization and then proceed to the classification of histology sections. We compare several different classification strategies to conclude that an autoencoder with softmax classifier provides the best performance.

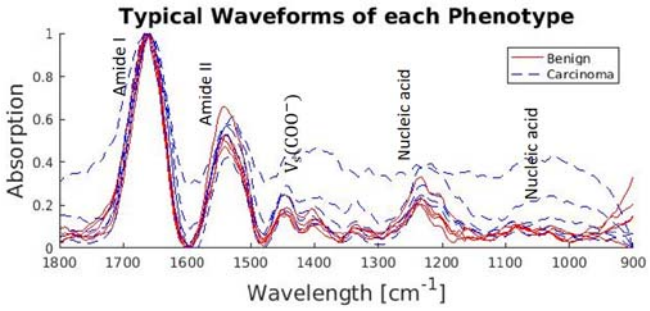

Figure 1: Randomly selected spectral signatures indicate (i) differentially expressed absorption levels between malignant and benign samples, and (ii) shift in the spectral peaks.

Organization of the paper is as follows. Section (II) summarizes previous research. Section (III) outlines the preprocessing steps for background correction. Section (IV) presents an approach to the visualization of hyperspectral

images. Section (V) outlines experimental design and performance of alternative methods for classification. Section (VI) concludes the paper.

2. PREVIOUS RESEARCH

QCL-IR can detect and identify functional groups of molecules in multicellular systems, and chemical differences have been explored for a number of tumor types. Due to the hyperspectral (e.g., high dimensionality) nature of images, specialized techniques for acquisition, preprocessing, and visualization have been developed and summarized in a recent review [10]. Although the review focuses on Raman microscopy, techniques are also applicable to QCL-IR. Most of the current tissue analytical techniques rely on dimensionality reduction followed by classification, and they have even been extended to the analysis of serum and blood [11, 12]. In one study, the outcome of patients with prostate cancer has been evaluated with FTIR imaging [13], where machine learning (e.g., feature selection, SVM) and risk scoring have been employed for improved predictive analysis. Their insights revealed that the stroma IR features could distinguish recurrence cases and have independent predictive power in combination with alternative methods. This is one of the first clinical studies that had constructed a significant cohort with the required clinical outcome for predictive modeling. In another recent study, benign and malignant phenotypes have been identified from tumor micro arrays (TMA) [14] using the random forest. A complete review of applications of IR spectroscopy for diagnostic of histology sections is outside of the scope of this paper; however, in the context of computational analysis, the bulk of previous research relies on factor analysis. In contrast to the previous research, we learned that linear methods of factor analysis do not produce an adequate performance for discriminant analysis for malignant versus benign tissues. As a result, alternative methods were evaluated to conclude spectral compression, via an autoencoder, followed by the softmax classifier provides adequate performance for a more extensive study.

3. PREPROCESSING

Preprocessing consists of 3 steps: (i) each tumor microarray (TMA) is first filtered to remove filters without any spectra. (ii) Baseline correction removes the low-frequency component of the spectral signatures. A number of methods have been proposed for background correction that includes (a) globally fitting a high order polynomial, or (b) locally rolling a ball over the spectra. A brief review of the prior art has been provided in [15]. Removal of the background is based on a regression model, with a rolling ball, fitting high order polynomial, or frequency analysis [15, 16]. In this paper, background correction is performed, per pixel, with a Matlab function that operates similarly to a rolling ball

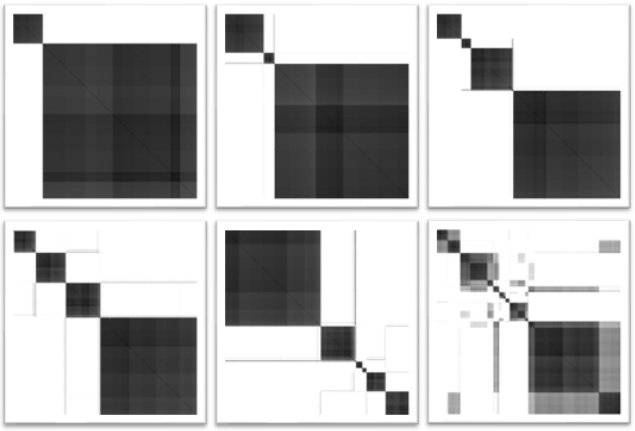

Figure 2: Consensus clustering reveals four stable clusters for benign samples. The number of clusters were varied from 2 to 7.

(e.g. fixed window). (iii) All spectra are normalized with respect to Amide I group to be equal to one.

4. VISUALIZATION

An initial exploration of the high dimensional spectral data with PCA and other methods of factor analysis did not produce adequate representation for visualization or classification. Furthermore, in this *pilot study*, we did not collect TMA samples that were specific to tumor or components of the stroma. Therefore, we examined the use of consensus clustering to identify stable clusters for each class of benign and malignant. In each class of benign or malignancy, five stable subtypes were identified with an example of benign subtypes shown in Figure 2. Each cluster represents a specific subset of bands and visualization for a subset of TMA is shown in Figure 3 by false coloring. The invasive and disorganized phenotypes of the malignant samples are partially visible in this image. On the other hand, the benign phenotypes appear to have a more organized cellular structure.

5. EXPERIMENTAL DESIGN AND CLASSIFICATION STRATEGIES

Twenty-two independent TMAs were sectioned at 10μm thick from paraffin-embedded blocks. They were mounted on two CaF2 discs, and the disks were imaged with a Spero®-QT microscope, from Daylight Solutions, with a pixel resolution of 4.3μm.

Three main approaches were explored and compared for classification: (i) autoencoder with softmax; (ii) decision trees; (iii) Convolutional Neural Network (CNN). Of the three methods, the autoencoder with softmax classifier performed the best, where the architecture is shown in Figure 4. Training was performed by increasing the number

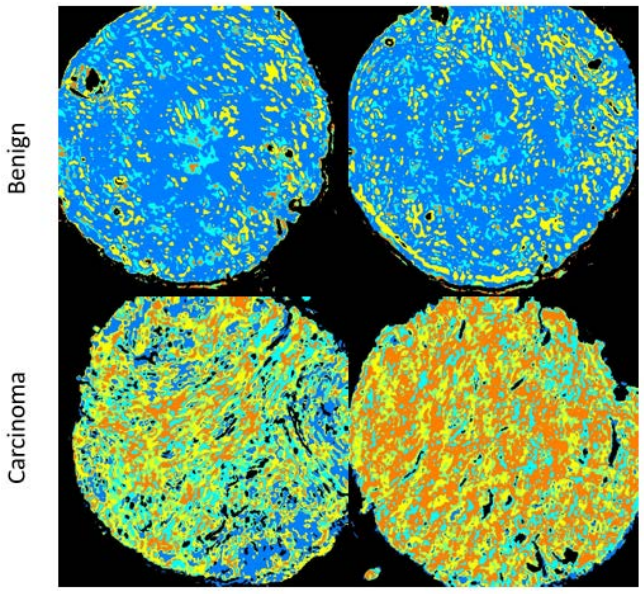

Figure 3: Chemical signatures of benign and malignant tissues are visualized by false colors, which are assigned to computed stable clusters.

of samples until the adequate performance was achieved. To start, *a single image* was used for training, while the rest were used for testing. Each test sample was then scored in terms of percentage of correct classification, and the sample with the worst score was added to the training set for the next iteration. This policy concluded that two samples from each class are sufficient for differentiating malignant and benign samples. Table 1 shows the classification results for each of the methodologies with one and two training samples per class. Subsequently, a label is assigned to each image by taking a majority vote of all labeled pixels, which yields a 100% classification accuracy in each of the three methods. However, the auto-encoder with softmax has classified more pixels correctly, in each image, when compared to other methods.

Since the autoencoder provided the best results, we opted for sensitivity analysis to determine the optimal number of nodes in the hidden layer. Figure 5 shows that the number of nodes in the hidden layer has little effect on classification, and the best is results are obtained with 22 nodes in the hidden layer. Overfitting is avoided since only 20% of the data is used for training, and there is not much of a deviation, in the performance, between training and testing data. With respect to CNN, several architectural settings were investigated for best performance. The best results were obtained by two convolutional layers each with five nodes and a convolutional kernel size of 100. This produced a total number of 140 features that are used as input to the softmax classifier layer. To prevent overfitting, dropout of the nodes during training was set to 50%.

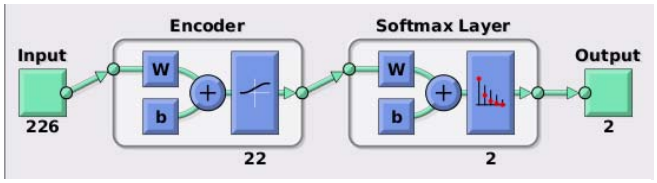

Figure 4: Autoencoder with softmax classifier provide superior performance.

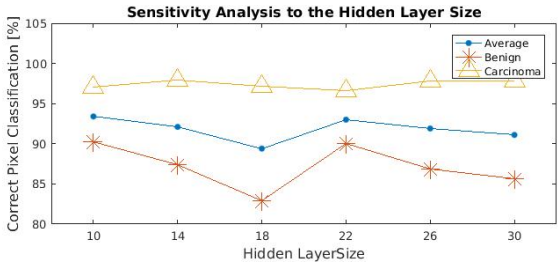

Figure 5: Sensitivity analysis indicates that performance is insensitive to number of nodes in the hidden layer.

Table 1: Comparison of alternative classification methods indicate improved performance for the autoencoder-softmax classifier.

	Training set of 2 images			Training set of 4 images		
	Decision Tree	CNN	Autoencoder	Decision Tree	CNN	Autoencoder
Benign	62.8	75.1	73.5	74.0	73.5	90
Carcinoma	86.2	82.1	86.5	93.5	94.4	96.6
Average	73.7	78.1	79.5	83.1	83.2	93.0

6. CONCLUSION AND DISCUSSION

Spectral histopathology is a promising approach for differentiating malignant phenotypes. Our results show that independent samples can be consistently labeled as benign or malignant using different classification strategies. However, the auto-encoder with softmax provided more stable results per image.

For malignant tissues, spectral data shows the same peaks (e.g., functional groups) that are also present in the benign tissues; however, in most cases, spectral peaks are either attenuated (e.g., protein Amide II) or eliminated in a small number of functional groups (e.g., nucleic acids, carbohydrates), or are shifted slightly. The range of the IR spectrum is associated with wavenumber for nucleic acids, phosphates, proteins, and glycogen. In a number of cases, the peak intensity has increased in malignant cases when compared to benign. For example, (i) the band intensity at 1258 cm^{-1}, corresponding to a nucleic acid sequence, has increased and shifted slightly to the right; and (ii) the protein spectra between 1543 – 1653 cm^{-1}, representing amide II have also appeared to increase for malignant cases. The backbone of Amide bonds is shown in Figure 6. Cancer cells have a higher metabolism; hence, resulting in higher protein synthesis and increased absorption level of the protein

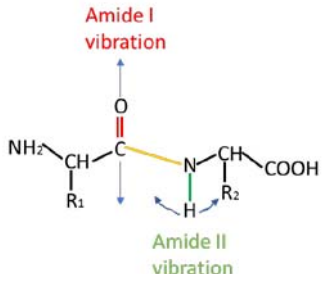

Figure 6: Chemical structure for the amide bond is shown, where R1 and R2 represents the side groups of amino acid. Because both the C=O and the N—H bonds are involved in the hydrogen bonding that takes place between the different elements of secondary structure, the locations of both the Amide I and Amide II bands are sensitive to the secondary structure content of a protein.

backbones of Amide II. In addition to the increased absorption level, there are no shifts in the spectral peaks of these two protein backbones. The shifts in the spectral peaks are associated either with the loss of hydrogen bonds (e.g., proteins coming apart) or increased number of hydrogen bonds in the backbone (e.g., protein folding). Thus, we conclude that there is no change in the protein conformation.

The main disadvantage of QCL-IR is a low spatial resolution. However, sample preparation is label-free, and the computational results show an effective classification performance by sampling hyperspectral signals of an image, training a model, and avoiding the use of spatial information. Accordingly, a simple model based on an encoder-decoder architecture with softmax classifier provides a more effective performance on an image-by-image basis. Our preliminary study concludes that diagnosis of breast cancer by QCL-IR is consistent using trained models in independent samples.

Acknowledgement: The authors thank Drs. Benjamin Bird and Bill Mohar of the Daylight Solutions for imaging the histology samples used in this study.

7. REFERENCES

[1] M. Veta, J. Pluim, P. van Diest, and M. Viergever, "Breast cancer histopathology image analysis: a review," *IEEE Transactions on Biomedical Engineering,* vol. 61, no. 5, pp. 1400-1411, 2014.

[2] M. T. McCann, J. A. Ozolek, C. A. Castro, B. Parvin, and J. Kovacevic, "Automated Histology Analysis [Opportunities for signal processing]," (in English), *IEEE Signal Processing Magazine,* vol. 32, no. 1, pp. 78-87, Jan 2015.

[3] M. Khoshdeli and B. Parvin, "Feature-based representation improves color decomposition and nuclear detection using convolutional neural network," *IEEE Transactions on Biomedical Engineering,* in press.

[4] M. Veta *et al.*, "Assessment of algorithms for mitosis detection in breast cancer histopathology images," *Medical Image Analysis,* vol. 20, no. 1, pp. 237-248, 2015.

[5] F. Xing and L. Yang, "Robust Nucleus/Cell Detection and Segmentation in Digital Pathology and Microscopy Images: A Comprehensive Review," *IEEE Rev Biomed Eng,* vol. 9, pp. 234-63, 2016.

[6] Y. Zhou, H. Chang, K. Barner, P. Spellman, and B. Parvin, "Classification of histology sections via multispectral convolutional sparse coding," in *CVPR*, Columbus, OH, 2014: IEEE.

[7] B. Bird and J. Rowlette, "High definition infrared chemical imaging of colorectal tissue using a Spero QCL microscope," *Analyst,* vol. 142, no. 8, pp. 1381-1386, Apr 10 2017.

[8] J. A. Kimber and S. G. Kazarian, "Spectroscopic imaging of biomaterials and biological systems with FTIR microscopy or with quantum cascade lasers," *Anal Bioanal Chem,* vol. 409, no. 25, pp. 5813-5820, Oct 2017.

[9] M. Pilling and P. Gardner, "Fundamental developments in infrared spectroscopic imaging for biomedical applications," *Chem Soc Rev,* vol. 45, no. 7, pp. 1935-57, Apr 07 2016.

[10] H. J. Butler *et al.*, "Using Raman spectroscopy to characterize biological materials," *Nat Protoc,* vol. 11, no. 4, pp. 664-87, Apr 2016.

[11] F. Elmi, A. F. Movaghar, M. M. Elmi, H. Alinezhad, and N. Nikbakhsh, "Application of FT-IR spectroscopy on breast cancer serum analysis," (in English), *Spectrochimica Acta Part a-Molecular and Biomolecular Spectroscopy,* vol. 187, pp. 87-91, Dec 5 2017.

[12] U. Zelig *et al.*, "Early detection of breast cancer using total biochemical analysis of peripheral blood components: a preliminary study," (in English), *Bmc Cancer,* vol. 15, May 15 2015.

[13] J. T. Kwak, A. Kajdacsy-Balla, V. Macias, M. Walsh, S. Sinha, and R. Bhargava, "Improving prediction of prostate cancer recurrence using chemical imaging," *Sci Rep,* vol. 5, p. 8758, Mar 04 2015.

[14] M. J. Pilling, A. Henderson, and P. Gardner, "Quantum Cascade Laser Spectral Histopathology: Breast Cancer Diagnostics Using High Throughput Chemical Imaging," *Anal Chem,* vol. 89, no. 14, pp. 7348-7355, Jul 18 2017.

[15] J. Han, S. Singh, L. Sun, B. Simmons, M. Auer, and B. Parvin, "Chemical profiling of the plant cellwall through Raman microspectroscopy," in *IEEE ISBI*, 2010.

[16] M. J. Baker *et al.*, "Using Fourier transform IR spectroscopy to analyze biological materials," *Nat Protoc,* vol. 9, no. 8, pp. 1771-91, Aug 2014.